

# Uniform Wafer-Scale Chemical Vapor Deposition of Graphene on Evaporated Cu (111) Film with Quality Comparable to Exfoliated Monolayer

Li Tao,<sup>†</sup> Jongho Lee,<sup>†</sup> Milo Holt,<sup>†</sup> Harry Chou,<sup>‡</sup> Stephen J. McDonnell,<sup>§</sup> Domingo A. Ferrer,<sup>†</sup> Matías G. Babenco,<sup>||</sup> Robert M. Wallace,<sup>§</sup> Sanjay K. Banerjee,<sup>†</sup> Rodney S. Ruoff,<sup>‡</sup> and Deji Akinwande<sup>\*†</sup>

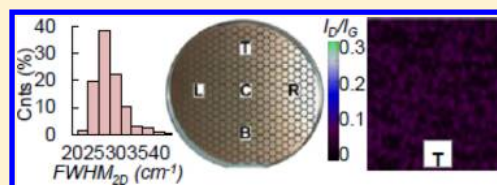
<sup>†</sup>Microelectronics Research Center, Department of Electrical Engineering, <sup>‡</sup>Department of Mechanical Engineering and the Texas Materials Institute, The University of Texas at Austin, Austin, Texas 78758, United States

<sup>§</sup>Department of Materials Science and Engineering, The University of Texas at Dallas, Richardson, Texas 75080, United States

<sup>||</sup>Department of Electrical Engineering, Universidad Nacional de Córdoba, Córdoba, Argentina

## S Supporting Information

**ABSTRACT:** This article demonstrated monolayer graphene grown on annealed Cu (111) films on standard oxidized 100-mm Si wafers with higher quality than existing reports. Large area Raman mapping indicated high uniformity (>97% coverage) of monolayer graphene with immeasurable defects (>95% defect-negligible) across the entire wafer. Key to these results is the phase transition of evaporated copper films from amorphous to (111) preferred crystalline, which resulted in subsequent growth of high quality graphene, as corroborated by X-ray diffraction and electron backscatter diffraction. Noticeably, such phase transition of the copper film was observed on a technologically ubiquitous Si wafer with a standard amorphous thermal oxide. A modified two-step etching transfer process was introduced to preserve the clean surface and electrical property of transferred monolayer graphene. The fabricated graphene field effect transistor on a flexible polyimide film achieved peak mobility over 4900 cm<sup>2</sup>/(V s) at ambient condition.



## INTRODUCTION

The wafer-scale synthesis of monolayer graphene with complete surface coverage and low defects for direct integration with standard complementary metal–oxide–semiconductor (CMOS) processes is a necessary requirement for very large-scale graphene nanoelectronics.<sup>1–6</sup> To this end, the Cu (111) surface has been identified as the preferred catalytic metal with a good lattice matching (lattice mismatch <4% at 300 °C) to graphene and is essential for achieving low defects with high uniformity.<sup>7–9</sup> However, Cu (111) films are typically obtained on single crystal epitaxial substrates such as sapphire,<sup>7,10</sup> which do not offer the low-cost and industrial scale processing of standard Si substrates. In contrast, copper films deposited on thermal oxides on Si (thus, SiO<sub>2</sub>/Si) are mostly amorphous as-deposited and usually form polycrystalline grains with random orientations after thermal treatment. Although the Cu (111) facet is energetically favorable considering its minimum surface energy compared to other facets,<sup>11,12</sup> it is not straightforward to obtain the (111) texture surface due to competing factors such as strain energy<sup>12,13</sup> and restricted boundaries.<sup>14,15</sup> The influence of these factors results in an increased fraction of (200),<sup>14</sup> or (220),<sup>15</sup> facets that are said to lead to nonuniform quality and substantial defects in the synthesized graphene.<sup>8</sup>

In this work, we report both the phase transition of evaporated amorphous copper to crystallized Cu (111) films on 100-mm SiO<sub>2</sub>/Si wafers after very high flow-rate H<sub>2</sub> thermal anneal at 900–1000 °C and growth of high quality graphene by

chemical vapor deposition (CVD) on this annealed substrate at wafer scale. Electron backscatter diffraction (EBSD) reveals that the crystallized copper film affords a (111) orientation in ~97% of the characterized surface, and X-ray diffraction (XRD) study verified that such crystallization occurs after high flow-rate H<sub>2</sub> annealing even before the graphene growth. This work scales the synthesis of high quality monolayer graphene on hydrogen enriched Cu (111) film<sup>16</sup> to 100-mm wafer size. Raman mapping of the CVD graphene shows high uniformity across the wafer with an average intensity ratio of the 2D-peak to G-peak ( $I_{2D}/I_G$ ) ~3.2, average full width at half-maximum of the 2D-peak ( $\text{fwhm}_{2D}$ ) ~30 cm<sup>-1</sup>, and very low defect density as measured by the D-peak to G-peak intensity ratio ( $I_D/I_G$ ) which is <0.2 for over 95% of the surface. Scanning tunneling microscopy (STM), transmission electron microscope (TEM), and electrical measurement all indicate that high quality graphene comparable to exfoliated graphene has been obtained.<sup>17,18</sup> These results pave the path for wafer-scale graphene nanotechnology with near-perfect monolayer coverage and with the material quality to afford the high-yield essential for very large-scale integrated systems.

Received: July 11, 2012

Revised: September 24, 2012

Published: October 24, 2012

## EXPERIMENTAL METHODS

**Graphene Synthesis.** As depicted in Figure 1, the synthesis procedure began from the electron-beam evaporation of 0.5–1

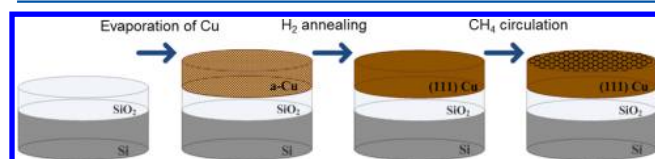


**Figure 1.** Process flow of chemical vapor deposition of graphene on evaporated Cu (111) film.

$\mu\text{m}$  copper (Plasmaterial, 99.99% pellets) film at  $10^{-6}$  Torr on a 300 nm  $\text{SiO}_2/\text{Si}$  wafer. The evaporated copper film sample was loaded with a quartz cap a few mm above (Supporting Information Figure S1) and annealed in a vertical cold-wall chamber (Aixtron Black Magic Nanoinstruments) under a hydrogen-saturated environment at a typical temperature of 975 °C for 5 min. Immediately after the annealing step, hydrogen was purged from the chamber, and ultrahigh purity methane (99.999% Matheson) with typical flow rates of 5–10 sccm was circulated for 5 min for graphene synthesis. After growth, the chamber was cooled from the growth temperature

to 550 °C at a rate of 50 °C/min in a gas-free environment. The heaters were then turned off, and cooling continued with 500 sccm of  $\text{N}_2$  gas. The samples were retrieved from the chamber at temperatures below 120 °C.

**Material Characterization.** A Renishaw In-Via Raman Microscope with He–Cd blue laser (442 nm wavelength) was employed to directly monitor the quality of graphene grown on the copper film.<sup>16</sup> Raman mapping data was analyzed and plotted using Graphene Raman Imaging and Spectroscopy Processing (GRISP) software (<https://nanohub.org/tools/grisp/>; authorization upon request) composed in MATLAB. Electron back scattering diffraction was performed on an EDAX/TSL OIM collection system attached to a Zeiss Neon 40 scanning electron microscope and analyzed with MATLAB for digitized inverted pole figure. X-ray diffraction was performed on a Philips X'Pert Pro X-ray system. A Veeco tapping-mode atomic force microscope was used for step analysis. A TECNAI G2 F20 X-TWIN transmission electron microscope was used for cross-sectional image of transferred graphene sandwiched between  $\text{SiO}_2/\text{Si}$  and epoxy.

**Graphene Transfer.** The graphene on a copper film was spun coated with 200 nm poly(methyl methacrylate) (PMMA) first and dried in vacuum (30 mbar) for 8 h. The copper film provides a smoother surface than foil, thus decreasing

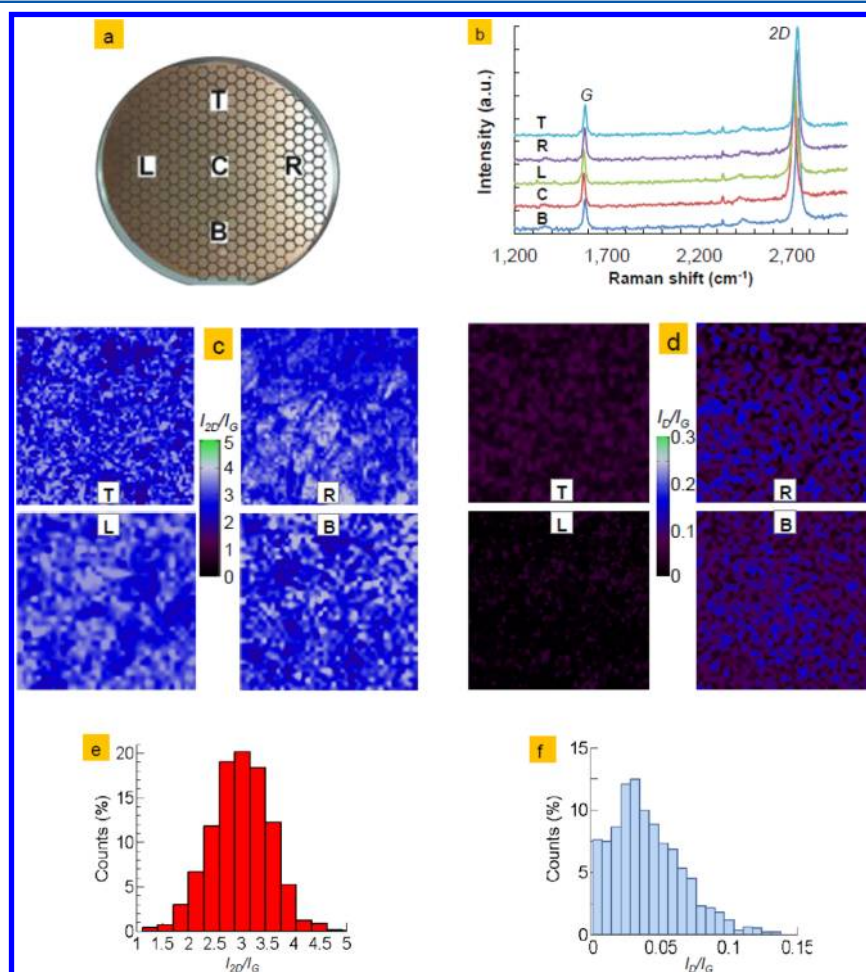


**Figure 2.** Raman characteristics of synthesized graphene: (a) Illustration of graphene on an optical image of Cu/ $\text{SiO}_2/\text{Si}$  100-mm wafer; (b) spot scans of 5 locations indicated on the wafer image: bottom (B), center (C), left (L), right (R) and top (T); (c and d) ratio maps of  $I_{2D}/I_G$  and  $I_D/I_G$  from Raman scan on 4 locations (scan size  $200 \times 200 \mu\text{m}^2$ ); (e and f) histograms showing monolayer graphene with an average  $I_{2D}/I_G \approx 3$ , and negligible D-peak (defects or disorder) with  $I_D/I_G < 0.2$  for over 95% of the scanned area.

Table 1. Comparison of Raman Signatures of Graphene Obtained with Various Methods

graphene obtained by various methods	fwhm <sub>2D</sub> (cm <sup>-1</sup> )	I <sub>2D</sub> /I <sub>G</sub>	I <sub>D</sub> /I <sub>G</sub>
this work on 100-mm wafer	25–35	2–4.5	0–0.2
CVD on deposited Cu or Ni film; (refs 1, 4, 29, 31, and 33)	30–36	2–4	0.2–0.4
CVD on cm-size copper foils (refs 8, 30, 32, 34, and 35)	27–35	2–4	<0.2
CVD/epitaxial			
on Cu (refs 7, 9, and 10)	30–40	1.5–2.5	0.05–1
on Co,Ni (refs 19, 23, 26, and 27)	30–40	0.3–3.3	~0.5
on Ru, Ir (refs 20–22 and 28)	42–46	~1	0.3–0.4
on SiC (refs 24 and 25)	37–50	~1	0.5–1
mechanical exfoliation (refs 17 and 18)	25–30	~4	<0.1

roughness induced wrinkles during transfer/multilayer stacking of the graphene film. The PMMA/graphene/Cu was then released from the SiO<sub>2</sub>/Si substrate after wet etching of SiO<sub>2</sub> in buffered oxide etchant (BOE, 6:1) and subsequently placed in an ammonium persulfate (APS) solution to etch the copper followed by deionized water cleaning. The cleaning was repeated for five more cycles. The floating PMMA/graphene film was then transferred onto the target substrate and vacuum-dried (30 mbar). Finally, the PMMA was dissolved away in a 50 °C acetone bath for ~30 min without a baking step.

**Device Fabrication.** The embedded gate was prepatterned on polyimide sheets by e-beam lithography (EBL) on PMMA and metal lift-off with 5 nm Ti plus 45 nm Pd or Au, followed by atomic deposition of 15 nm Al<sub>2</sub>O<sub>3</sub> as gate dielectrics. After the transfer of graphene onto the prepatterned polyimide substrate, the channel region was defined with EBL followed by oxygen plasma etching at 50 W, 200 mTorr for 50 s. At last, source and drain contacts were formed by EBL and metal lift-off with 5 nm Ti plus 45 nm Pd to complete the device fabrication. All EBL work here was performed on a JEOL 6000 e-beam machine at 50 kV on 200 nm thick PMMA that is coated with conductive polymer E-SPACER 300Z.

## RESULTS AND DISCUSSION

Typical synthesis process in this study, as depicted in Figure 1, included a saturated hydrogen annealing step, a growth step with ultrahigh purity methane only, and a two-step cooling before unloading samples from a vertical cold-wall chamber with separate shower head and substrate heaters (see the Graphene Synthesis section). The saturated hydrogen annealing step before the growth of graphene was found to be critical for achieving the results reported in this work, as discussed further below. There are few key changes made in the growth configuration and parameters to obtain uniform high quality graphene shown in our previous result on centimeter square pieces to 100-mm wafers. First, the temperature control was switched from pyrometer feedback for small pieces to thermocouple feedback for wafer-scale samples, giving better real-time and accurate control of the growth temperature. Second, the ramping rate of the top heater was recalibrated to match the bottom heater in order to maintain uniform and stable temperature across 100-mm wafers. The two improvements highlighted above address the accuracy, stability, and uniformity of temperature that are crucial for the high quality of synthesized graphene. Another important parameter is the thickness of the Cu film which was increased to 1–1.5 μm for wafer scale samples compared to 500 nm for small pieces due to greater mass loss for a large area Cu film at high temperature under vacuum (see the Supporting Information Figure S1 and S2 for experimental details regarding wafer-scale synthesis).

Immediately after the synthesis of graphene, the sample was characterized with a Raman spectroscopy using a blue laser as the light source (see the Material Characterization section). Raman spectra from five spot-locations over a 100-mm diameter wafer as denoted in Figure 2a (B for bottom, C for center, L for left, R for right, and T for top, respectively) are presented in Figure 2b. The average fwhm<sub>2D</sub> in Figure 2b is ~28 cm<sup>-1</sup>, with I<sub>2D</sub>/I<sub>G</sub> ≈ 3, and no measurable D-peak signifying the successful growth of high-quality monolayer graphene. To verify the uniformity of the synthesized graphene, Raman maps across 200 × 200 μm<sup>2</sup> areas were obtained with each centered on the locations (B, R, L, and T) mentioned above, and evaluated as I<sub>2D</sub>/I<sub>G</sub> and I<sub>D</sub>/I<sub>G</sub> ratio maps in Figure 2, panels c and d, respectively. User-interface software named GRISP was created for rapid extraction of ratio maps and histogram plots from large data files (see the Supporting Information Figure S3 and S4). It is worth noting here that the rainbow scale for Raman maps shown here is for more vivid visualization. The uniformity of these signatures can be more accurately judged from statistical data such as histograms that more precisely quantify the growth uniformity. For instance, the histogram data in Figure 2, panels e and f, indicate average values of 3.2 ± 0.19 for I<sub>2D</sub>/I<sub>G</sub> and that >95% of the scanned area has I<sub>D</sub>/I<sub>G</sub> < 0.2. Based on the statistical data from Raman mapping data, monolayer graphene has been achieved on a 100-mm wafer scale with negligible or no measurable defects. The Raman growth results here are of higher quality in terms of the I<sub>D</sub>/I<sub>G</sub> and fwhm<sub>2D</sub>, and also offer cost and scale advantages, compared to those achieved with epitaxial copper on expensive non-Si substrates.<sup>7,9,10</sup> Raman signatures of the graphene in this work are compared in Table 1 to those for graphene obtained by other methods.<sup>1,4,7–10,17–35</sup>

The successful synthesis of uniform monolayer graphene with negligible disorder depends on using a hydrogen-enriched evaporated Cu (111) film as first report in our previous study.<sup>16</sup> A high percentage (over 96.8% in a 1 × 1 mm<sup>2</sup> area) for a Cu (111) orientation was observed by EBSD mapping (Figure 3a) after annealing and then graphene synthesis. This distinguishes the evaporated copper film reported here from conventional copper foils, which show a Cu (100) orientation as the dominant facet after the same CVD process.<sup>16</sup> XRD data in Figure 3b further indicates that this dominant (111) orientation formed immediately after the hydrogen annealing step and before the growth of graphene. Cu (111) surface offers some advantages for growing high quality graphene relative to other facets as also observed in other reports.<sup>7,8,14,15</sup> A microscopic route for graphene growth on copper catalytic surface includes (i) adsorption of precursor such as CH<sub>4</sub> and its decomposition into carbon monomer/dimer,<sup>36–38</sup> (ii) the diffusion of carbon monomers/dimers leading to the formation of clusters,<sup>37,38</sup> and (iii) the attachment (growth) or detachment (etching) of

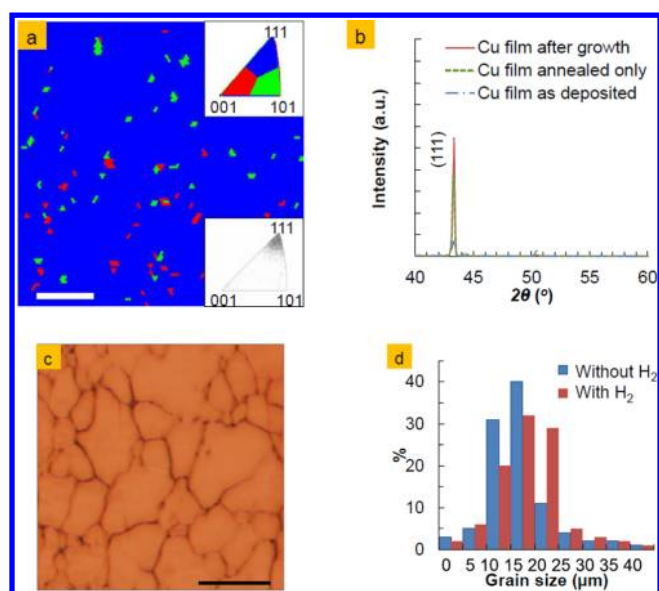


**Figure 3.** (a) Electron backscatter diffraction mapping revealing the dominant Cu (111) crystal orientation after graphene growth (scale bar = 200  $\mu\text{m}$ ). The insets are the inverse pole legend (top) and raw data (bottom); (b) X-ray diffraction of copper film as deposited, annealed only and after the growth of graphene. The dominant orientation observed after growth is Cu (111) at  $2\theta \sim 43.3^\circ$ ; (c) optical image (scale bar = 20  $\mu\text{m}$ ) showing copper grains with an average size  $\sim 18 \mu\text{m}$ ; (d) histograms of copper grain size with and without  $\text{H}_2$  flow during graphene growth.

carbon at the edge of existing cluster/nuclei. First, the adsorption energy for the initial steps of decomposing  $\text{CH}_4$  on Cu (111) is lower than other facets.<sup>36,37</sup> Second, the diffusion rate of a carbon monomer/dimer on Cu (111) is higher than other facets like Cu (100).<sup>8,37</sup> In addition, the Cu (111) surface offers less nuclei density and a faster growth rate<sup>38</sup> for graphene grains than other crystal facets, which altogether could yield large graphene domains under the conditions reported here and even at temperatures  $\leq 900^\circ\text{C}$ .<sup>16</sup>

The negligible or weak D-peak intensity in the Raman spectroscopy of graphene grown on Cu (111) film is likely due to fewer defects. It has been previously reported that the root causes of defects monitored by the D-peak in the Raman spectroscopy of otherwise clean graphene can be attributed to two kinds of imperfections that break translational symmetry: (i) graphene domains or grain boundaries with mixed zigzag (ZZ) and arm-chair (AC) edges<sup>39–41</sup> and/or (ii) the boundary between graphene and imperfect catalytic surface or underlying substrate.<sup>8,42,43</sup> Recent density functional theory (DFT) modeling of the Cu (111) surface suggested that the dominant growing edge of graphene should be in the ZZ direction.<sup>44–46</sup> The absence of AC edges was considered to be because of their rapid passivation by copper atoms.<sup>46</sup> Graphene domains terminated by ZZ edges show no or negligible D-peak in the Raman spectra, whereas grain boundaries with combined AC and ZZ edges will induce a significant D-peak intensity.<sup>40</sup> For this reason, the polycrystalline graphene on evaporated copper film observed in this work should have infinitesimal portion of AC edges based on the negligible D-peak observed in the

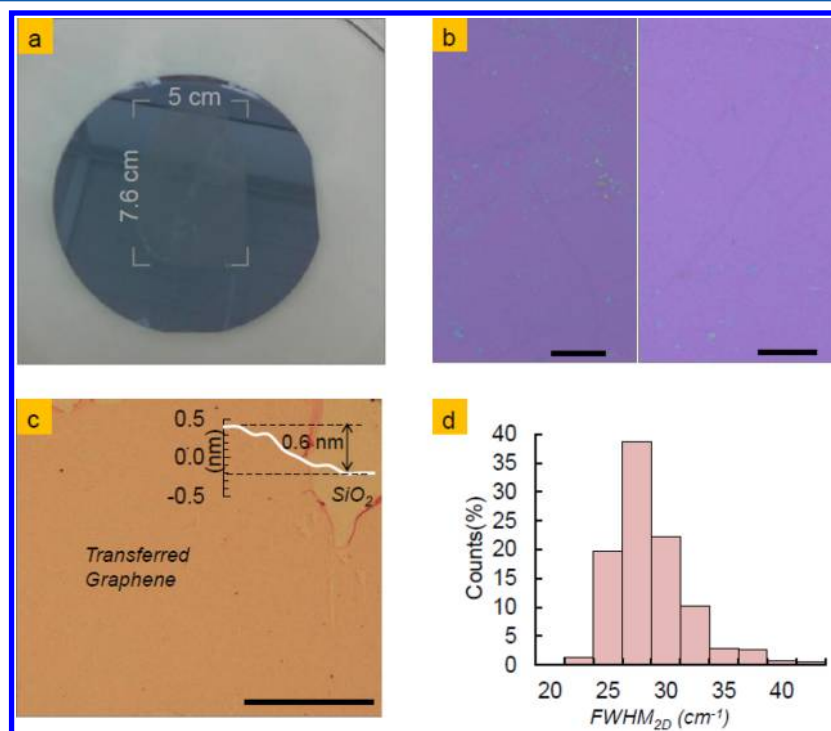


**Figure 4.** (a) PMMA/Graphene film ( $\sim 5 \times 7.6 \text{ cm}^2$ ) floating above a target 100-mm wafer during transfer process; (b) Graphene film transferred onto  $\text{SiO}_2/\text{Si}$  substrate: the left-hand side sample has undergone post-transfer baking at  $150^\circ\text{C}$  for 30 min before PMMA removal with acetone while the right-hand side sample was directly soaked in a  $50^\circ\text{C}$  acetone bath to remove PMMA (scale bar = 10  $\mu\text{m}$ ). The former method results in a visibly larger concentration of PMMA residue; (c) Optical microscope image of graphene on  $\text{SiO}_2/\text{Si}$ , showing uniform contrast over  $0.5 \times 0.5 \text{ mm}^2$  area (scale bar = 200  $\mu\text{m}$ ). The inset is the step height measurement by atomic force microscopy in an open region in the film exposing the underlying  $\text{SiO}_2$ ; (d) histogram of the  $\text{fwhm}_{2D}$  from Raman mapping over  $200 \times 200 \mu\text{m}^2$  area (96.3% of collected data points has  $\text{fwhm}_{2D}$  of 25–35  $\text{cm}^{-1}$ ).

Raman spectroscopy. From the growth kinetics point of view, there is a reason that lower defect level could be obtained on the Cu film reported here. As seen from the shape of the graphene domains captured during short-time growths, 3-fold and 6-fold symmetry growth fronts are observed (see the Supporting Information Figure S5). Both of these two shapes could form a seamless match with hexagonal lattice compared to 2 or 4 fold observed elsewhere, leading to less structural defects. Six-fold edges has been reported to be most likely ZZ terminated,<sup>41</sup> which yields less defects as aforementioned and also agrees with our observation in this study.

Another important synthesis feature is the role of H<sub>2</sub> on the annealed Cu (111) film which contrasts with conventional foils. Owing to the higher adsorption of hydrogen on Cu (111) than other crystal orientations,<sup>47–49</sup> a significant amount of hydrogen can adsorb and diffuse into the Cu (111) film during hydrogen saturation annealing.<sup>16</sup> The absorbed hydrogen can subsequently diffuse to the film surface to serve as a cocatalyst for monolayer graphene growth,<sup>35</sup> thereby eliminating the need for a gas-phase H<sub>2</sub> precursor during the growth step, which can result in graphene etching with a noticeable D-peak.<sup>16,50</sup> On the other hand, the presence of hydrogen during the growth process likely contributes to an increase in the average copper grain size owing to increased surface mobility. For instance, the average grain size of ~15–20 μm obtained without H<sub>2</sub> can further be increased to 20–25 μm with H<sub>2</sub> precursor during growth as shown in Figure 3, panels c and d.

Samples with a graphene monolayer synthesized on copper film using the route reported here, albeit on a limited size scale (~5 × 7.6 cm<sup>2</sup>, Figure 4a), have been transferred to various substrates such as SiO<sub>2</sub>/Si, quartz, and flexible polyimide sheets via a two-step etching procedure (see the Graphene Transfer section). In this transfer procedure, the PMMA/graphene/Cu film stack was first released from SiO<sub>2</sub>/Si wafer through SiO<sub>2</sub> etching. Then, the film stack was floated on the etchant solution with the entire backside of Cu film exposed. Consequently, the etching time for this evaporated copper film is greatly reduced (~5 min) compared to conventional copper foils that are more than an order of magnitude thicker. In our transfer process, the PMMA was dissolved away in a 50 °C acetone bath for ~30 min without a post-transfer baking step that alleviate residues of PMMA on the graphene surface (Figure 4b) commonly reported in the literature.<sup>51,52</sup> Figure 4c shows an optical image (scope size of 0.5 × 0.5 mm<sup>2</sup> limited by the lens) of clean graphene that has been transferred onto a standard 300-nm thick SiO<sub>2</sub>/Si with our two-step transfer process. A typical thickness of the graphene layer is ~0.6 nm measured by atomic force microscopy (AFM). The histogram of the fwhm of the Raman 2D peak (Figure 4d) indicates the transferred film is monolayer graphene which agrees with aforementioned Raman characteristics. STM image of graphene on the copper film prior to the transfer (Figure 5a) and high resolution cross-sectional TEM image of the transferred graphene (Figure 5b) further confirm that the graphene film was monolayer throughout the whole process. A current challenge with PMMA assisted transfer is the undesired polymer residue that remains on the graphene surface even after solvent cleaning and thermal baking (see the Supporting Information Figure S6).<sup>52</sup> Addressing this challenge is a future scientific task.

High quality graphene monolayer on copper film was also transferred to polyimide plastic sheets,<sup>53</sup> using the two-step etching wet-transfer, for the fabrication of flexible graphene

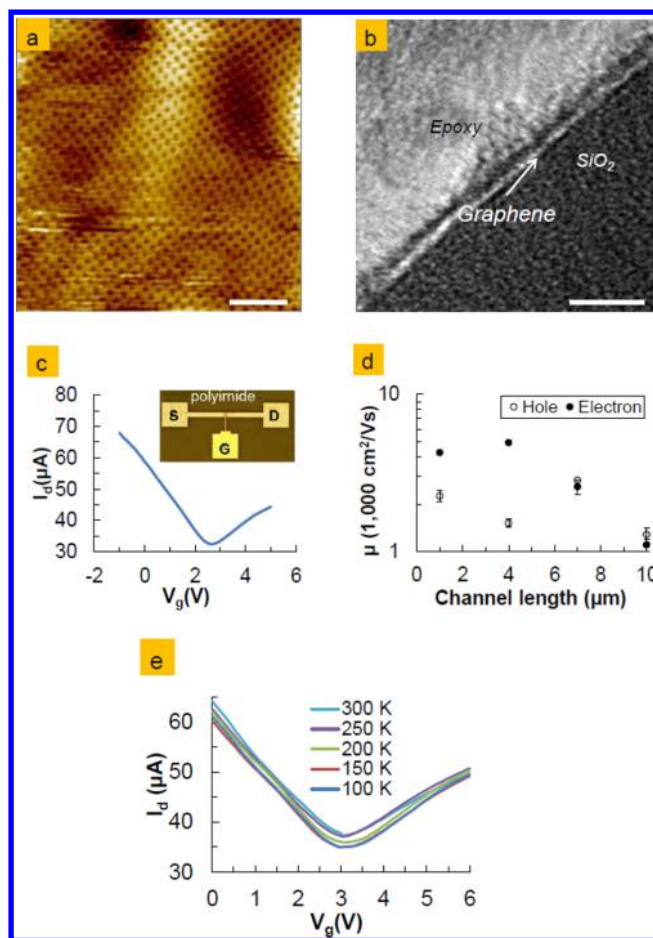


**Figure 5.** (a) Monolayer hexagonal lattice of the as-grown graphene on copper film confirmed by scanning tunneling microscopy (scale bar = 2 nm); (b) cross-sectional transmission electron microscope image indicates that the graphene transferred onto SiO<sub>2</sub>/Si substrate is monolayer of good structural quality (scale bar = 5 nm); (c) representative  $I_d$ - $V_g$  curve from graphene field effect transistors with  $V_d = 100$  mV measured at ambient condition; and (d) mobility dependence on the channel length. An average mobility is ~2000 cm<sup>2</sup>/(V s) with peak value of 4930 cm<sup>2</sup>/(V s), which was 5–10 times higher than most reported mobility values for graphene field effect transistors on a flexible/plastic substrate; (e)  $I_d$ - $V_g$  curve as a function of measurement temperature ranging from 100 to 300 K with 50 K increments under vacuum of ~10<sup>-6</sup> mbar.

field-effect transistors (GFET). The device fabrication followed the procedure in the Device Fabrication section. Electrical characterization of the embedded-gate GFETs was performed at ambient condition on a Cascade probe station with Agilent B1500 semiconductor device analyzer, and exhibited the typical V-shape profile in the  $I_D$ - $V_G$  (Figure 5c). The hole mobility varied within 50% of 2000 cm<sup>2</sup>/(V s) for an order of magnitude length scale. Increased mobility for electron was generally observed with shorter channel (Figure 5d), indicative of less scattering of the charge carriers. A peak mobility of ~4900 cm<sup>2</sup>/(V s) had been obtained at room temperature and pressure as in our previous report,<sup>53</sup> which is 5–10 times larger than previously reported values for GFETs fabricated directly on flexible substrates.<sup>54,55</sup> This relatively high field effect mobility at ambient condition arise from two aforementioned aspects: (1) better intrinsic graphene quality synthesized here and (2) the improved transfer process providing cleaner interface between graphene and metal or dielectrics. A relatively modest

Dirac voltage in Figures 5c also suggests weak impurity doping of the transferred graphene from polymer residue. A thick residue of PMMA will result in much higher Dirac voltage.<sup>52</sup> The mobility and transport characteristics of the flexible GFETs was also found to be relatively insensitive to, temperatures ranging from 100 to 300 K as seen in Figure 5e.

## SUMMARY AND CONCLUSION

In summary, chemical vapor deposition of high quality monolayer graphene on copper film evaporated onto 100-mm SiO<sub>2</sub>/Si wafers has been demonstrated. Analytical results derived from Raman mapping data across the wafer via homemade software, GRISP, suggest uniform graphene with negligible defects. STM, cross-sectional TEM and AFM measurement further confirm the high quality monolayer graphene. The high quality uniform wafer-scale monolayer synthesized in this study is a consequence of unique hydrogen-rich annealed Cu (111) films as corroborated by EBSD and XRD. A two-step etching based transfer of the graphene film is realized and high quality monolayer character of the graphene is intact after the transfer process. Compared to conventional copper foils, this approach has the potential for direct integration with standard CMOS processes either using a transfer-free process<sup>29</sup> or by direct bonding to a target substrate which is currently a matter of further research. The quality of the synthesized graphene on copper film achieved in this work exceeds that from epitaxial copper substrates and is comparable to exfoliated graphene but with scalability beyond the reach of exfoliation methods.

## ASSOCIATED CONTENT

### Supporting Information

- (1) Experimental details in wafer-scale synthesis of graphene.
- (2) Graphene Raman Imaging and Spectroscopy Processing (GRISP) software.
- (3) Growth study of graphene on Cu film.
- (4) Graphene film after transfer and Figures S1–S6 referred in the main text. This material is available free of charge via the Internet at <http://pubs.acs.org>.

## AUTHOR INFORMATION

### Corresponding Author

\*E-mail: [deji@ece.utexas.edu](mailto:deji@ece.utexas.edu). Tel: 512-471-4345. Fax: 512-232-2893.

### Notes

The authors declare no competing financial interest.

## ACKNOWLEDGMENTS

The authors thank A. Lee, Dr. Y. Hao, and Dr. H. Li for insightful discussions. Graphene synthesis was performed in an Aixtron Black Magic system. This work is supported in part by the Nanoelectronic Research Initiative (NRI SWAN Center) and the Office of Naval Research under the program of Dr. Chagaan Baatar.

## REFERENCES

- (1) Su, C.-Y.; Lu, A.-Y.; Wu, C.-Y.; Li, Y.-T.; Liu, K.-K.; Zhang, W.; Lin, S.-Y.; Juang, Z.-Y.; Zhong, Y.-L.; Chen, F.-R. *Nano Lett.* **2011**, *11*, 3612–3616.
- (2) Yamaguchi, H.; Eda, G.; Mattevi, C.; Kim, H.; Chhowalla, M. *ACS Nano* **2010**, *4*, 524–528.
- (3) Liu, N.; Fu, L.; Dai, B.; Yan, K.; Liu, X.; Zhao, R.; Zhang, Y.; Liu, Z. *Nano Lett.* **2010**, *11*, 297–303.

- (4) Lee, Y.; Bae, S.; Jang, H.; Jang, S.; Zhu, S.-E.; Sim, S. H.; Song, Y. I.; Hong, B. H.; Ahn, J.-H. *Nano Lett.* **2010**, *10*, 490–493.
- (5) Kim, K.; Choi, J.-Y.; Kim, T.; Cho, S.-H.; Chung, H.-J. *Nature* **2011**, *479*, 338–344.
- (6) Jinseong, H.; Hyun-Jong, C.; Sung-Hoon, L.; Heejun, Y.; Jaikwang, S.; Chung, U. I.; Sunae, S. *Device Res. Conf. (DRC)* **2011**, 31–32.
- (7) Hu, B.; Ago, H.; Ito, Y.; Kawahara, K.; Tsuji, M.; Magome, E.; Sumitani, K.; Mizuta, N.; Ikeda, K.-i.; Mizuno, S. *Carbon* **2011**, *50*, 57–65.
- (8) Wood, J. D.; Schmucker, S. W.; Lyons, A. S.; Pop, E.; Lyding, J. W. *Nano Lett.* **2011**, *11*, 4547–4554.
- (9) Gao, L.; Guest, J. R.; Guisinger, N. P. *Nano Lett.* **2010**, *10*, 3512–3516.
- (10) Reddy, K. M.; Gledhill, A. D.; Chen, C.-H.; Drexler, J. M.; Padture, N. P. *Appl. Phys. Lett.* **2011**, *98*, 113117.
- (11) Thompson, C. V. *Annu. Rev. Mater. Sci.* **1990**, *20*, 245–268.
- (12) Weinhacht, V.; Brückner, W. *Thin Solid Films* **2002**, *418*, 136–144.
- (13) Thompson, C. V.; Carel, R. *J. Mech. Phys. Solids* **1996**, *44*, 657–673.
- (14) Brongersma, S. H.; Kerr, E.; Vervoort, I.; Maex, K. *AIP Conference Proc.* **2002**, *612*, 229.
- (15) Chen, K. N.; Fan, A.; Tan, C. S.; Reif, R.; Wen, C. Y. *Appl. Phys. Lett.* **2002**, *81*, 3774–3776.
- (16) Tao, L.; Lee, J.; Chou, H.; Holt, M.; Ruoff, R. S.; Akinwande, D. *ACS Nano* **2012**, *6*, 2319–2325.
- (17) Ferrari, A. C.; Meyer, J. C.; Scardaci, V.; Casiraghi, C.; Lazzeri, M.; Mauri, F.; Piscanec, S.; Jiang, D.; Novoselov, K. S.; Roth, S. *Phys. Rev. Lett.* **2006**, *97*, 187401.
- (18) Graf, D.; Molitor, F.; Ensslin, K.; Stampfer, C.; Jungen, A.; Hierold, C.; Wirtz, L. *Nano Lett.* **2007**, *7*, 238–242.
- (19) Gamo, Y.; Nagashima, A.; Wakabayashi, M.; Terai, M.; Oshima, C. *Surf. Sci.* **1997**, *374*, 61–64.
- (20) N'Diaye, A. T.; Bleikamp, S.; Feibelman, P. J.; Michely, T. *Phys. Rev. Lett.* **2006**, *97*, 215501.
- (21) Marchini, S.; Günther, S.; Wintterlin, J. *Phys. Rev. B* **2007**, *76*, 075429.
- (22) Sutter, P. W.; Flege, J.-I.; Sutter, E. A. *Nat. Mater.* **2008**, *7*, 406–411.
- (23) Usachov, D.; Dobrotvorskii, A. M.; Varykhalov, A.; Rader, O.; Gudat, W.; Shikin, A. M.; Adamchuk, V. K. *Phys. Rev. B* **2008**, *78*, 085403.
- (24) Emtsev, K. V.; Bostwick, A.; Horn, K.; Jobst, J.; Kellogg, G. L.; Ley, L.; McChesney, J. L.; Ohta, T.; Reshanov, S. A.; Rohrl, J. *Nat. Mater.* **2009**, *8*, 203–207.
- (25) Robinson, J. A.; Wetherington, M.; Tedesco, J. L.; Campbell, P. M.; Weng, X.; Stitt, J.; Fanton, M. A.; Frantz, E.; Snyder, D.; VanMil, B. L. *Nano Lett.* **2009**, *9*, 2873–2876.
- (26) Ago, H.; Ito, Y.; Mizuta, N.; Yoshida, K.; Hu, B.; Orofeo, C. M.; Tsuji, M.; Ikeda, K.-i.; Mizuno, S. *ACS Nano* **2010**, *4*, 7407–7414.
- (27) Iwasaki, T.; Park, H. J.; Konuma, M.; Lee, D. S.; Smet, J. H.; Starke, U. *Nano Lett.* **2010**, *11*, 79–84.
- (28) Sutter, P. W.; Albrecht, P. M.; Sutter, E. A. *Appl. Phys. Lett.* **2010**, *97*, 213101.
- (29) Levendorf, M. P.; Ruiz-Vargas, C. S.; Garg, S.; Park, J. *Nano Lett.* **2009**, *9*, 4479–4483.
- (30) Li, X.; Magnuson, C. W.; Venugopal, A.; Tromp, R. M.; Hannon, J. B.; Vogel, E. M.; Colombo, L.; Ruoff, R. S. *J. Am. Chem. Soc.* **2011**, *133*, 2816–2819.
- (31) Reina, A.; Jia, X.; Ho, J.; Nezich, D.; Son, H.; Bulovic, V.; Dresselhaus, M. S.; Kong, J. *Nano Lett.* **2008**, *9*, 30–35.
- (32) Li, X.; Zhu, Y.; Cai, W.; Borysiak, M.; Han, B.; Chen, D.; Piner, R. D.; Colombo, L.; Ruoff, R. S. *Nano Lett.* **2009**, *9*, 4359–4363.
- (33) Ismach, A.; Druzgalski, C.; Penwell, S.; Schwartzberg, A.; Zheng, M.; Javey, A.; Bokor, J.; Zhang, Y. *Nano Lett.* **2010**, *10*, 1542–1548.
- (34) Li, X.; Magnuson, C. W.; Venugopal, A.; An, J.; Suk, J. W.; Han, B.; Borysiak, M.; Cai, W.; Velamakanni, A.; Zhu, Y. *Nano Lett.* **2010**, *10*, 4328–4334.

- (35) Vlassioun, I.; Regmi, M.; Fulvio, P.; Dai, S.; Datskos, P.; Eres, G.; Smirnov, S. *ACS Nano* **2011**, *5*, 6069–6076.
- (36) Gajewski, G.; Pao, C.-W. *J. Chem. Phys.* **2011**, *135*, 064707–064709.
- (37) Zhang, W.; Wu, P.; Li, Z.; Yang, J. *J. Phys. Chem. C* **2011**, *115*, 17782–17787.
- (38) Kim, H.; Mattevi, C.; Calvo, M. R.; Oberg, J. C.; Artiglia, L.; Agnoli, S.; Hirjibehedin, C. F.; Chhowalla, M.; Saiz, E. *ACS Nano* **2012**, *6*, 3614–3626.
- (39) Casiraghi, C.; Hartschuh, A.; Qian, H.; Piscanec, S.; Georgi, C.; Fasoli, A.; Novoselov, K. S.; Basko, D. M.; Ferrari, A. C. *Nano Lett.* **2009**, *9*, 1433–1441.
- (40) Krauss, B.; Nemes-Incze, P. t.; Skakalova, V.; Biro, L. s. P.; Klitzing, K. v.; Smet, J. H. *Nano Lett.* **2010**, *10*, 4544–4548.
- (41) Yu, Q.; Jauregui, L. A.; Wu, W.; Colby, R.; Tian, J.; Su, Z.; Cao, H.; Liu, Z.; Pandey, D.; Wei, D. *Nat. Mater.* **2011**, *10*, 443–449.
- (42) Rasool, H. I.; Song, E. B.; Allen, M. J.; Wassei, J. K.; Kaner, R. B.; Wang, K. L.; Weiller, B. H.; Gimzewski, J. K. *Nano Lett.* **2010**, *11*, 251–256.
- (43) Zhao, L.; Rim, K. T.; Zhou, H.; He, R.; Heinz, T. F.; Pinczuk, A.; Flynn, G. W.; Pasupathy, A. N. *Solid State Commun.* **2011**, *151*, 509–513.
- (44) Saadi, S.; Abild-Pedersen, F.; Helveg, S.; Sehested, J.; Hinnemann, B.; Appel, C. C.; Nørskov, J. K. *J. Phys. Chem. C* **2010**, *114*, 11221–11227.
- (45) Wu, P.; Zhang, W.; Li, Z.; Yang, J.; Hou, J. G. *J. Chem. Phys.* **2010**, *133*, 071101–071104.
- (46) Shu, H.; Chen, X.; Tao, X.; Ding, F. *ACS Nano* **2012**, *6*, 3243–3250.
- (47) Strömquist, J.; Bengtsson, L.; Persson, M.; Hammer, B. *Surf. Sci.* **1998**, *397*, 382–394.
- (48) Kammler, T.; Küppers, J. *J. Chem. Phys.* **1999**, *111*, 8115–8123.
- (49) Thomsen, L.; Onsgaard, J.; Godowski, P. J.; Møller, P.; Hoffmann, S. V. *J. Vac. Sci. Technol., A* **2001**, *19*, 1988–1992.
- (50) Losurdo, M.; Giangregorio, M. M.; Capezzuto, P.; Bruno, G. *Phys. Chem. Chem. Phys.* **2011**, *13*, 20836–20843.
- (51) Liang, X.; Sperling, B. A.; Calizo, I.; Cheng, G.; Hacker, C. A.; Zhang, Q.; Obeng, Y.; Yan, K.; Peng, H.; Li, Q. *ACS Nano* **2011**, *5*, 9144–9153.
- (52) Pirkle, A.; Chan, J.; Venugopal, A.; Hinojos, D.; Magnuson, C. W.; McDonnell, S.; Colombo, L.; Vogel, E. M.; Ruoff, R. S.; Wallace, R. M. *Appl. Phys. Lett.* **2011**, *99*, 122108–122103.
- (53) Lee, J.; Tao, L.; Hao, Y.; Ruoff, R. S.; Akinwande, D. *Appl. Phys. Lett.* **2012**, *100*, 152104–152104.
- (54) Nayfeh, O. M. *IEEE Electron Device Lett.* **2011**, *32*, 1349–1351.
- (55) Kim, B. J.; Jang, H.; Lee, S.-K.; Hong, B. H.; Ahn, J.-H.; Cho, J. H. *Nano Lett.* **2010**, *10*, 3464–3466.